Article

# Low-cost and effective fabrication of biocompatible nanofibers from silk and cellulose-rich materials

Susana Guzman-Puyol, José Alejandro Heredia-Guerrero, Luca Ceseracciu, Hadi Hajiali, Claudio Canale, Alice Scarpellini, Roberto Cingolani, Ilker S. Bayer, Athanassia Athanassiou, and Elisa Mele

## Just Accepted

1 # Low-cost and effective fabrication of biocompatible nanofibers from

2 # silk and cellulose-rich materials

3

4 Susana Guzman-Puyol[a,*], José A. Heredia-Guerrero[a], Luca Ceseracciu[a], Hadi Hajiali[a,b], Claudio

5 Canale[c], Alice Scarpellini[d], Roberto Cingolani[a,c,d], Ilker S. Bayer[a], Athanassia Athanasiou[a,*], Elisa

6 Mele [a,†,*]

7

8 [a] *Smart Materials, Istituto Italiano di Tecnologia, Via Morego, 30, Genova, 16163, Italy*

9 [b] *DIBRIS, University of Genoa, Via Opera Pia, 13, Genova, 16145, Italy*

10 [c] *Nanophysics, Istituto Italiano di Tecnologia, Via Morego, 30, Genova, 16163, Italy*

11 [d] *Nanochemistry, Istituto Italiano di Tecnologia, Via Morego, 30, Genova, 16163, Italy*

12

13 E-mail addresses: susana.guzman@iit.it, athanassia.athanasiou@iit.it, e.mele2@lboro.ac.uk

14

15 [†] *Present address: Department of Materials, Loughborough University, Loughborough,*

16 *Leicestershire, LE11 3TU, UK*

17

## Abstract

19 Here, we show the production of nanofibrous mats with controlled mechanical properties and

20 excellent biocompatibility by combining fibroin with pure cellulose and cellulose-rich parsley

21 powder agro-waste. To this end, trifluoroacetic acid was used as common solvent for all the

22 involved biomaterials, achieving highly homogeneous blends that were suitable for the

23 electrospinning technique. Morphological analysis revealed that the electrospun composite

24 nanofibers were well-defined and defect-free, with a diameter in the range of 65-100 nm.

25 Mechanical investigations demonstrated that the fibrous mats exhibited an increased stiffness when

1

26    pure fibroin was combined with cellulose, whereas they possessed an increased flexibility when the

27    parsley waste was added to fibroin. Lastly, the produced mats were highly biocompatible, as

28    demonstrated by the promoted proliferation of fibroblast cells. The characteristics of the hybrid

29    fibroin-cellulose nanofibers, in terms of nanoscale topography, mechanical properties and

30    biocompatibility, are attractive and potentially applicable in the biomedical sector.

31

## **Introduction**

33    Fibroin and cellulose are two biomaterials often found in natural fibrillary structures because they

34    provide structural support and mechanical resistance that are crucial for the vital functions of insects

35    and plants [1]. In particular, the fibroin microfibrils are structural components of the silk produced

36    by spiders and silkworms [2]. The fibers of the silkworm *Bombyx Mori* cocoon, for instance, are

37    formed by two filaments of fibroin, held together by a matrix of sericin [3], Figure 1A. The

38    orientation and crystalline structure of the fibroin domains confer to these fibers high mechanical

39    strength and extensibility that is important to provide protection to the silkworm pupae from

40    external threats [4]. On the other hand, in the vegetable kingdom, cellulose microfibrils are the main

41    building blocks of plant cell walls. They are mainly constituted by oriented (1,4)-linked $\beta$-D glucan

42    chains that are embedded in a matrix of polysaccharides, such as pectin and hemicelluloses [5],

43    Figure 1B. Cellulose microfibrils are stiff enough to protect plant cells from environmental stresses

44    and to resist to the internal turgor pressure during cell growth and expansion [6].
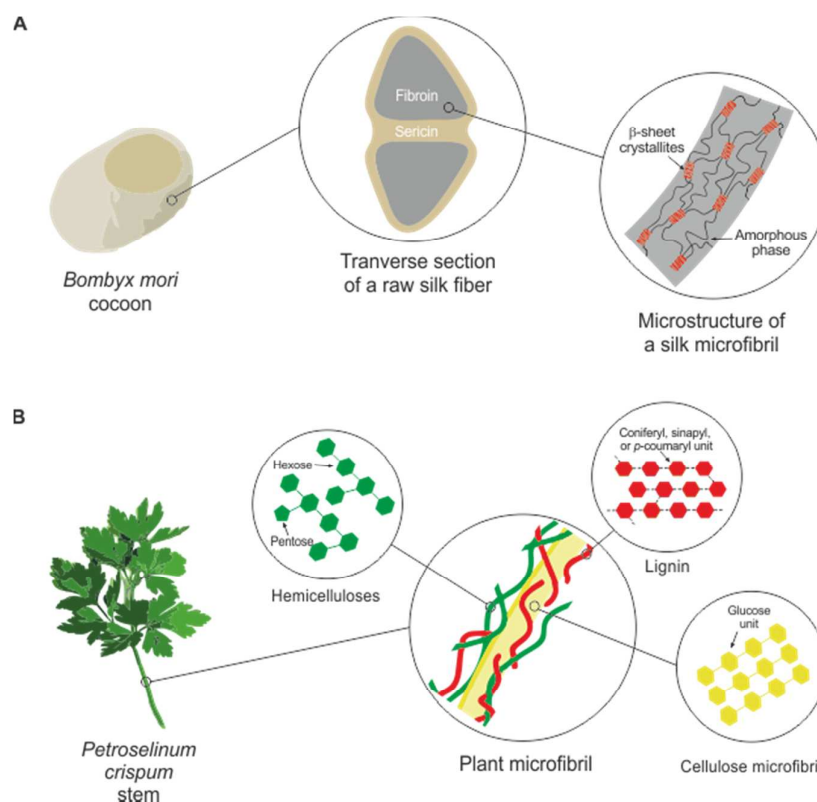
**Figure 1.** Schematic of the main components of (A) *Bombyx mori* cocoon and (B) parsley stem residues, and relative organization at different scales.

The excellent mechanical properties of both fibroin and cellulose materials, together with their biocompatibility and biodegradability, have fostered the development of strategies able to effectively use these two biopolymers to create novel composite systems with applications in different sectors [7,8]. In particular, films with tunable mechanical performances and controlled water stability have been prepared starting from homogeneous ionic-liquid solutions of fibroin and cellulose [9-11]. These films have been used to direct the chondrogenesis of mesenchymal stem cells [10] and to promote the proliferation of fibroblasts [11]. Moreover, other solvents, such as aqueous cuprammonium hydroxide [12-14] and N-methylmorpholine oxide [15], have been use to blend both those biopolymers and to form films. In each case, an interaction between fibroin and cellulose has been observed. Furthermore, microfibers with a diameter ranging between 15 and 40 μm have been fabricated by wet [16,17] and dry spinning [18,19] of fibroin-cellulose blends. On the contrary, to the best of our knowledge, to date no attempts have been reported on the production of

61 fibroin-cellulose blend nanofibers (diameter in the submicron range), despite the increasing

62 attention that these nanostructures are gaining in regenerative medicine [20].

63 A technology that is of particular interest for this research area is electrostatic spinning (ES),

64 because it allows to fabricate nanofibrous mats and scaffolds with the desired biophysical,

65 biochemical and biomechanical properties [21]. The nanoscale topography and the three-

66 dimensional (3D) interconnected porosity of the electrospun constructs have been used to control

67 cell proliferation, migration and differentiation [22,23]. Furthermore, a variety of biocompatible and

68 biodegradable, synthetic and natural materials can be processed by ES, including fibroin [24-27]. In

69 fact, electrospun nanofibers of this protein and its combination with other biopolymers, such as

70 poly(ethylene oxide), poly(L-lactic acid-co-ε-caprolactone), chitosan, and collagen, have been

71 proposed for the regeneration of blood vessels and nerves [28,29]. Previous works on ES of fibroin

72 have reported the use of water, ionic liquids, hexafluoroisopropanol or hexafluoroacetone hydrate

73 as solvents [30-33].

74 In this paper, we show that hybrid nanofibers of fibroin (from *Bombyx mori* silkworm cocoons) and

75 microcrystalline cellulose or cellulose-rich parsley waste can be electrospun using trifluoroacetic

76 acid (TFA) as common solvent, without the need of additives or subsequent treatments. In

77 particular, mats of well-defined and defect-free nanofibers were produced by combining fibroin

78 with pure cellulose or dried powder of parsley (*Petroselinum crispum*) stems at a 1:1 ratio. The

79 physicochemical characterization of the samples revealed that the different constituents were well

80 distributed inside the nanofibers without segregation or phase separation effects. The addition of

81 cellulose to fibroin allowed the production of stiffer mats. Interestingly, nanofibers containing

82 parsley exhibited an elastic modulus comparable to that of the fibroin fibers but with a higher

83 elongation at maximum load. Furthermore, all the nanofibrous supports were highly biocompatible,

84 promoting the adhesion and proliferation of fibroblasts. The use of dried parsley stems as source of

85 cellulose demonstrated that valuable products can be obtained even from vegetable waste, rich in

86 cellulose, through the here discussed procedure. Furthermore, *Petroselinum crispum* is an herb of

4

87   interest for biomedical applications, because it contains bioactive compounds, including

88   antioxidants, anticancer and anti-inflammatory molecules [34-36].

89

## Materials and methods

**Materials and cell line**

92   *Bombyx mori* silkworm cocoons used in this research were purchased from Angkorchum Trading

93   Inc. In order to remove sericin, raw silk was degummed using a 0.02 M solution of $Na_2CO_3$ in

94   boiling water for 30 minutes. Degummed silk fibers were then washed thoroughly with deionized

95   water to remove any remaining sericin and rest of surfactants, and then dried in air overnight. After

96   degumming and drying, raw silk lost about 25% of its original weight. High purity microcrystalline

97   cellulose (MCC, crystallinity ~79%) from cotton linters and anhydrous TFA were purchased from

98   Sigma Aldrich and used as received. Dried powder of parsley (*Petroselinum crispum*) stems was

99   provided by a vegetable producer (Ida S.r.l., Italy) as not edible food waste.

100   For the biocompatibility assay, Dulbecco's Modified Eagle's Medium (DMEM), Bovine Calf Serum

101   (BCS), trypsin–EDTA solution, penicillin-streptomycin, Phosphate Buffered Saline (PBS),

102   fuoroshield with DAPI and thiazolyl blue tetrazolium bromide (MTT) were purchased from Sigma

103   Aldrich. Alexa Fluor® 488 phalloidin was from Life Technology. Fibroblast cells from murine

104   embryo (NIH3T3-cells) were obtained from ATCC® (CRL-1658™).

105

**Fabrication of the electrospun nanofibers**

107   Solutions for electrospinning were prepared by separately dissolving fibroin, MCC and dried

108   parsley powder in TFA at a concentration of 3% w/w. The procedure described in Ref. [37] was

109   followed for cellulose and parsley solutions. Briefly, cellulose solutions were obtained by

110   dissolving MCC in TFA for 3 days under shaking, whereas the dissolution of pulverized parsley

111   stems took 28 days under shaking, and of fibroin just few seconds.  Then, the fibroin solution was

112    mixed with the MCC or the parsley solution at 1:1 volume ratio, in order to have MCC:fibroin or

113    parsley:fibroin blends, respectively. Other combinations of MCC:fibroin and parsley:fibroin were

114    also prepared but they were not suitable for the ES process producing particles instead of fibers or

115    fibers with a high number of beads. For this reason we selected the combination 1:1 volume ratio.

116    For the ES process, a syringe with a stainless-steel 23-gauge needle was filled with the polymer

117    solution (fibroin, MCC:fibroin or parsley:fibroin) and connected to a syringe pump (NE-1000, New

118    Era Pump Systems, Inc.) working at a constant flow rate of 1 mL/hour. The needle was clamped to

119    the positive electrode of a high-voltage power supply generating 18 kV, and an aluminum disk

120    (diameter 50 mm, thickness 3 mm) rotating at a speed of 2500 rpm was used as collector (needle-

121    collector distance of 15 cm). The ES experiments were conducted by means of the high speed roto-

122    translating electrospinning system of Linari Engineering (RT Collector Web).

123

**Morphological characterization**

125    High-resolution Scanning Electron Microscopy (SEM) imaging was carried out using a JEOL JSM

126    7500FA (Jeol, Tokyo, Japan) equipped with a cold field-emission gun (FEG), operating at 15 kV

127    acceleration voltage. The samples were coated with a 10 nm thick film of carbon using an Emitech

128    K950X high vacuum turbo system (Quorum Technologies Ltd, East Sussex - UK). Imaging was

129    performed with the secondary electrons to analyze the morphology of the fibers. The fibers'

130    diameter was calculated with ImageJ image analyzer program. Basically, the SEM images were

131    loaded into the software and diameter of the fibers was measured using a two point measuring

132    analysis. Approximately, 100 measurements were taken to obtain the diameter distribution of each

133    type of fibers.

134

**Chemical and structural characterization**

136    Infrared spectra were obtained with an Attenuated Total Reflectance (ATR) accessory (MIRacle

137    ATR, PIKE Technologies) coupled to a Fourier Transform Infrared (FTIR) spectrometer (Equinox

6

138 70 FT-IR, Bruker). All spectra were recorded in the range from 4000 to 600 cm$^{-1}$ with a resolution

139 of 4 cm$^{-1}$, accumulating 128 scans. Measurements were performed on nanofibers of fibroin,

140 MCC:fibroin and parsley:fibroin, and on films of cellulose and parsley after treatment with TFA. To

141 assess the homogeneity of chemical composition, ATR-FTIR spectra were recorded three times on

142 different samples. Deconvolution of amide I components (1720-1580 cm$^{-1}$) was carried out by using

143 of PeakFit 4.11 software. In order to remove the contribution of cellulose or parsley in this spectral

144 region, spectra of such components were subtracted by the mixtures' spectra by previous

145 normalization respect to C-O stretching of polysaccharides (*ca.* 1016 cm$^{-1}$ for cellulose and 1022

146 cm$^{-1}$ for parsley). Wavenumber positions of components were deduced by calculation of the second-

147 order derivative. Deconvolution was performed using Gaussian shape with an amplitude threshold

148 of 3%. A non-linear least-square method was employed to reduce the differences between the

149 calculated spectra and the original one. The crystalline structure of nanofibers was analyzed by X-

150 ray diffraction (XRD) using a diffractometer Rigaku SmartLab X-Ray Diffractometer equipped

151 with a copper rotating anode. The X-ray source was operated at 40 kV and 150 mA. A Gobel mirror

152 was used to obtain a parallel beam and to suppress Cu Kβ radiation (1.392 Å). The measurements

153 were performed using a 2$\theta$ scan.

154

155 **Thermal characterization**

156 The thermal degradation behavior of the nanofibers was investigated by a standard

157 thermogravimetric analysis (TGA) method using a TGA Q500 from TA Instruments. Measurements

158 were performed on 3-5 mg of samples in an aluminum pan under inert $N_2$ atmosphere with a flow

159 rate of 50 mL/min at a temperature range from 30 to 600°C and a heating rate of 5°C/min. The

160 weight loss and its first derivative were recorded simultaneously as a function of time/temperature.

161

162 **Mechanical characterization**

7

163    The mechanical properties of mats were obtained by uniaxial tension tests on a dual column

164    universal testing machine (Instron 3365). Mats were cut in prismatic specimen with a width of 4

165    mm and an effective length of 25 mm. In order to avoid accidental damage during handling,

166    specimens were tested with the paper frame method, already reported in Ref. [38]; briefly, the

167    samples were first taped on custom made paper frames composed by two detachable halves, then

168    mounted on the testing machine's hydraulic clamps. Displacement was applied with the rate of 2

169    mm/min. From the resulting stress strain curves, the apparent elastic modulus, ultimate tensile

170    strength (UTS), elongation at yield and elongation at maximum load were extracted. The term

171    "apparent" refers to the fact that the measured value is not an intrinsic property of the bulk material,

172    but depends on the mat density and structure. Measurements were performed on 5 samples per each

173    material. All the stress-strain curves were recorded at 25 °C and 44% relative humidity (RH).

174    Single-fiber mechanical characterization was performed in a liquid environment of phosphate-

175    buffered saline (PBS) by atomic force microscope (AFM) by a Nanowizard III (JPK Instruments,

176    Germany) mounted on an Axio Observer D1 (Carl Zeiss, Germany) inverted optical microscope. V-

177    shaped DNP silicon nitride cantilevers (Bruker, Massachussets, US) with a nominal spring constant

178    0.24 N/m, resonance frequency in air ranging from 40 kHz to 75 kHz and tip typical curvature

179    radius of >20 nm were used. The actual spring constant of each cantilever was determined *in situ*

180    using the thermal noise method [39]. Images were acquired in quantitative imaging (QI) mode, a

181    recently developed imaging mode based on force measurements [40]. A maximum force of 7 nN

182    was applied on the sample and 256×256 force-distance (FD) curves were acquired per each image.

183    Then, FD curves were converted into force-indentation (FI) and the stiffness was extracted from the

184    curves slope.

185

**Biocompatibility study**

187    NIH3T3 cells were cultured in DMEM supplemented with 10% of BCS and 1% of antibiotics (100

188    U/mL penicillin and 0.1 mg/mL streptomycin), in incubator at 37 °C with 5% $CO_2$. The culture

189  medium was replaced every 3 days. The electrospun samples were sterilized under ultraviolet (UV)

190  light for 30 minutes, and subsequently they were washed using a PBS solution. Fibroblast cells

191  were detached from the culture flask using trypsin-EDTA solution, when 80% of confluence was

192  reached, and seeded onto the electrospun mats. Adhered and proliferated cells, cultured for 24

193  hours, were analysed by a colorimetric MTT assay. In order to observe the morphology of cells, the

194  samples were fixed in 3.7% formaldehyde for 15 min before rinsing them with PBS for 3 times.

195  Samples were then permeabilized with 1% Triton X-100, and stained with alexa-fluor 488

196  phalloidin and DAPI for actin cytoskeleton and nucleus, respectively. The confocal microscope

197  Nikon A1 was utilized to visualize the morphology of fluorescent-stained 3T3 fibroblasts on the

198  electrospun fibres.

199

## **Results and discussion**

201  **Morphological characterization**

202  The SEM images in Figure 2A show that electrospinning fibroin from TFA solutions resulted in

203  well-defined nanofibers without defects or beads. The analysis of the fiber population in the mat

204  demonstrated a predominance of fibers having a size in the range of 50-120 nm (72% of the total

205  population, Figure 2D). The calculated average diameter was of $(103\pm25)$ nm. When fibroin

206  solution was blended with MCC or parsley waste solution (1:1 ratio), the use of TFA as common

207  solvent promoted the miscibility of the polymers, without inducing phase separation before the ES

208  process. This positively affected the morphology of the produced composite fibers that were free

209  from beaded structures, as visible in Figure 2B and 2C for MCC:fibroin and parsley:fibroin,

210  respectively. In both cases, the average diameter of the fibers decreased of about 37% with respect

211  to pure fibroin, being $(65\pm11)$ nm and $(64\pm12)$ nm for MCC:fibroin (Figure 2E) and parsley:fibroin

212  (Figure 2F) nanofibers, respectively. The majority of the population (approximately 70%) was

213  characterized by a size in the range of 50-70 nm, and no fibers had a diameter larger than 180 nm.
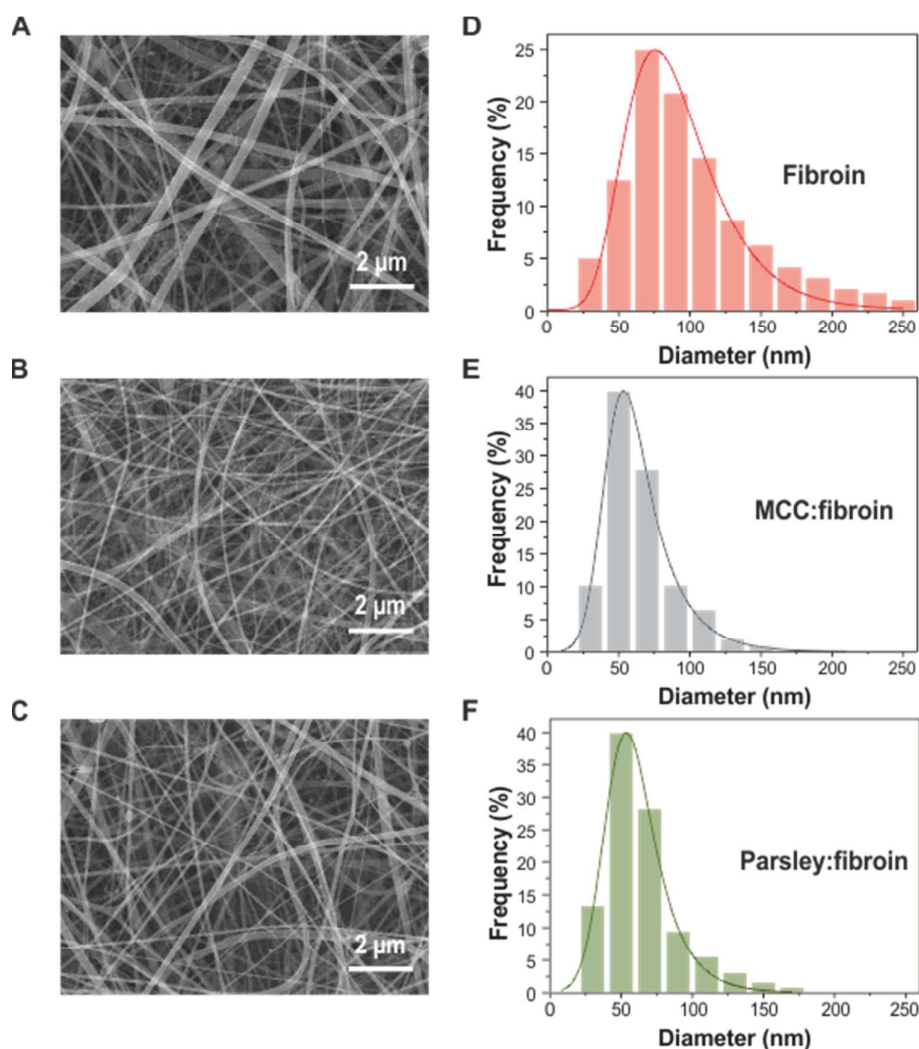
214

215

**Figure 2.** SEM images of the electrospun nanofibers: (A) fibroin, (B) MCC:fibroin and (C) parsley:fibroin. Histograms showing the width distribution of the nanofibers: (D) fibroin, (E) MCC:fibroin and (F) parsley:fibroin.

219

220

221 **Chemical, structural and thermal characterization**

222 The chemical characterization of fibroin, MCC:fibroin, and parsley:fibroin nanofibers was carried

223 out by ATR-FTIR. As shown in Figure 3A, the samples are characterized by the presence of

224 vibrations associated with fibroin (amide A –hydrogen-bonded NH stretching– at 3279 cm$^{-1}$, amide

225 B –NH Fermi resonance– at 3074 cm$^{-1}$, amide I –C=O stretching– at 1640 cm$^{-1}$, amide II –in-plane

226 N-H bending coupled to C-N stretching– at 1515 cm$^{-1}$, and amide III –similarly to amide II, in-

227 plane N-H bending coupled to C-N stretching– at 1236 cm$^{-1}$) [41,42]. Moreover, characteristic

228 bands of cellulose (OH stretching at 3354 cm$^{-1}$, CH stretching at 2889 cm$^{-1}$, adsorbed water at 1643

229    cm$^{-1}$, ring breathing at 1155 cm$^{-1}$, and C-O stretching at 1016 cm$^{-1}$) [43] or parsley (OH stretching

230    at 3294 cm$^{-1}$, asymmetric and symmetric CH$_2$ stretching of lipid molecules at 2918 and 2851 cm$^{-1}$,

231    respectively, C=C stretching of lignin at 1672 cm$^{-1}$, and C-O stretching of polysaccharides at 1022

232    cm$^{-1}$) [37] can be observed. No traces of TFA were detected. However, small modifications of the

233    shape of amide I and II absorptions in the spectra of MCC:fibroin and parsley:fibroin samples with

234    respect to the fibroin one were observed. Usually, such differences are ascribed to changes of the

235    secondary structure of the fibroin that were quantified by deconvolution of amide I vibration [44],

236    Figure 3B. Amide I components are shown in Figure S1 (supplementary information). For fibroin

237    nanofibers main contribution was associated with random coils, while β-sheets and turns were

238    lightly smaller. Minor fractions were side chains and α-helices. These results are consistent with Ha

239    et al. (2006) [45] who stated that regenerated fibroin from TFA solutions shows random coil and β-

240    sheet characteristics. In the case of MCC:fibroin also random coil was the main component and

241    turns and α-helices increased their values at the expense of β-sheets and side chains, while

242    parsley:fibroin sample presented a pattern of contributions very similar to pure fibroin.
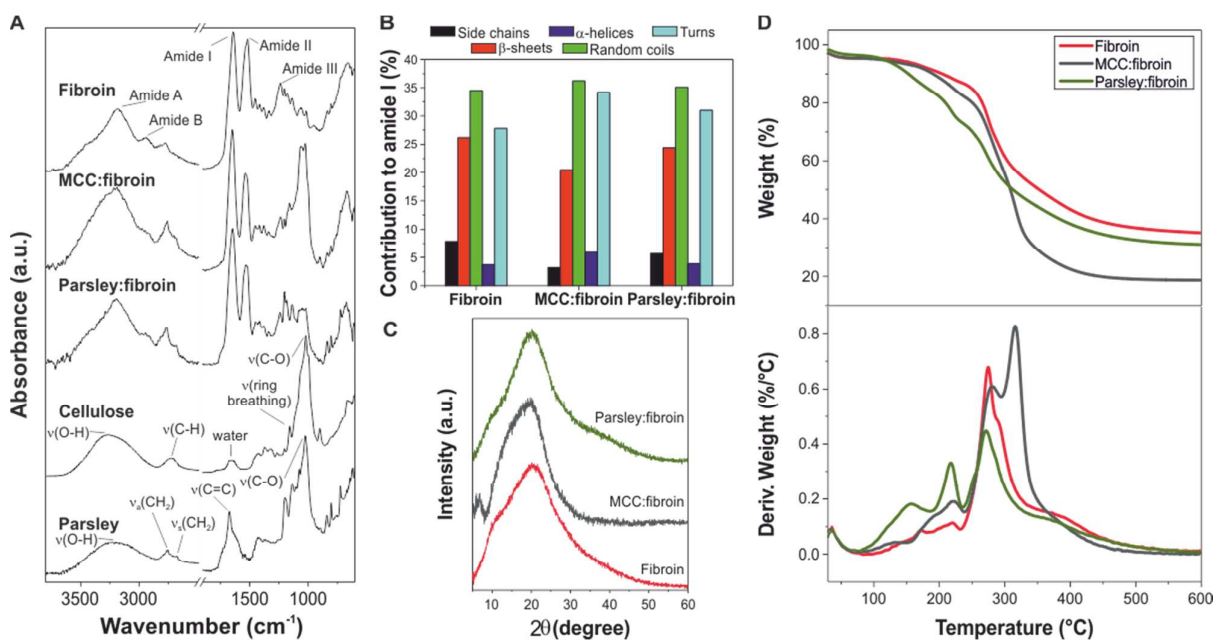
243



244

**Figure 3.** (A) ATR-FTIR spectra of the electrospun nanofibers. (B) Contribution to amide (%) from deconvolution of the amide I region of the ATR-FTIR spectra. (C) XRD patterns of the electrospun nanofibers. (D) TGA thermograms and derivative thermogravimetric curves of the electrospun nanofibers.

The diffractograms in Figure 3C displayed a broad halo centered around 20-21° for all types of nanofibers. This can be ascribed to a strong amorphous character of cellulose or parsley components after TFA treatment [37], according with ATR-FTIR data but also to the amorphous contribution of silk fibroin [46].

The thermal properties of fibroin, MCC:fibroin and parsley:fibroin nanofibers were examined by TGA. TGA thermograms and the corresponding derivative curves are shown in Figure 3D top and bottom, respectively. A region of weight loss for temperature values up to 100 °C was observed for all the samples and it was due to the loss of water (environmental humidity) absorbed by the electrospun mats. Fibroin nanofibers (red curve) exhibited a second region of weight loss between 270 and 380 °C with a peak at 274 °C that was associated with the degradation of amino acid side groups and cleavage of peptide bonds [47,48]. On the other hand, MCC:fibroin nanofibers (grey curve) showed two main thermal events at 280 and 316 °C, being ascribed to the degradation of fibroin and cellulose fraction, respectively. In fact, pure cellulose films prepared using TFA as solvent present a single well-defined thermal degradation peak at 326 °C [37]. Finally, the thermogram of parsley:fibroin nanofibers (green curve) was characterized by three main peaks at 157, 217 and 271 °C. The first two peaks can be attributed to the parsley fraction, whereas the third peak is related to the juxtaposition of the main degradation peaks of fibroin and parsley. As previously reported in literature, bioplastics prepared from parsley stem residues have a first weight loss at 144 °C, a second at 219 °C, and a third one at 277 °C, ascribed to the existence of diverse organic components [37].

**Mechanical characterization**

271    Typical stress-strain curves of each type of nanofibers are reported in Figure 4A. Two different

272    behaviors can be noticed: fibroin and MCC:fibroin mats present a short slack recovery, followed by

273    a classical Hookean linear deformation, and by yield and plastic deformation. Parsley:fibroin

274    samples, instead, exhibit a nonlinear deformation behavior with an initial large deformation at low

275    load, followed by a quick increment of stiffness. The elastic modulus, ultimate tensile strength

276    (UTS), strain at yield and elongation at maximum load extracted from such curves are reported in

277    Table 1 and in Figure 4B. For parsley:fibroin nanofibers, the elastic moduli associated with both

278    regions are reported.

279
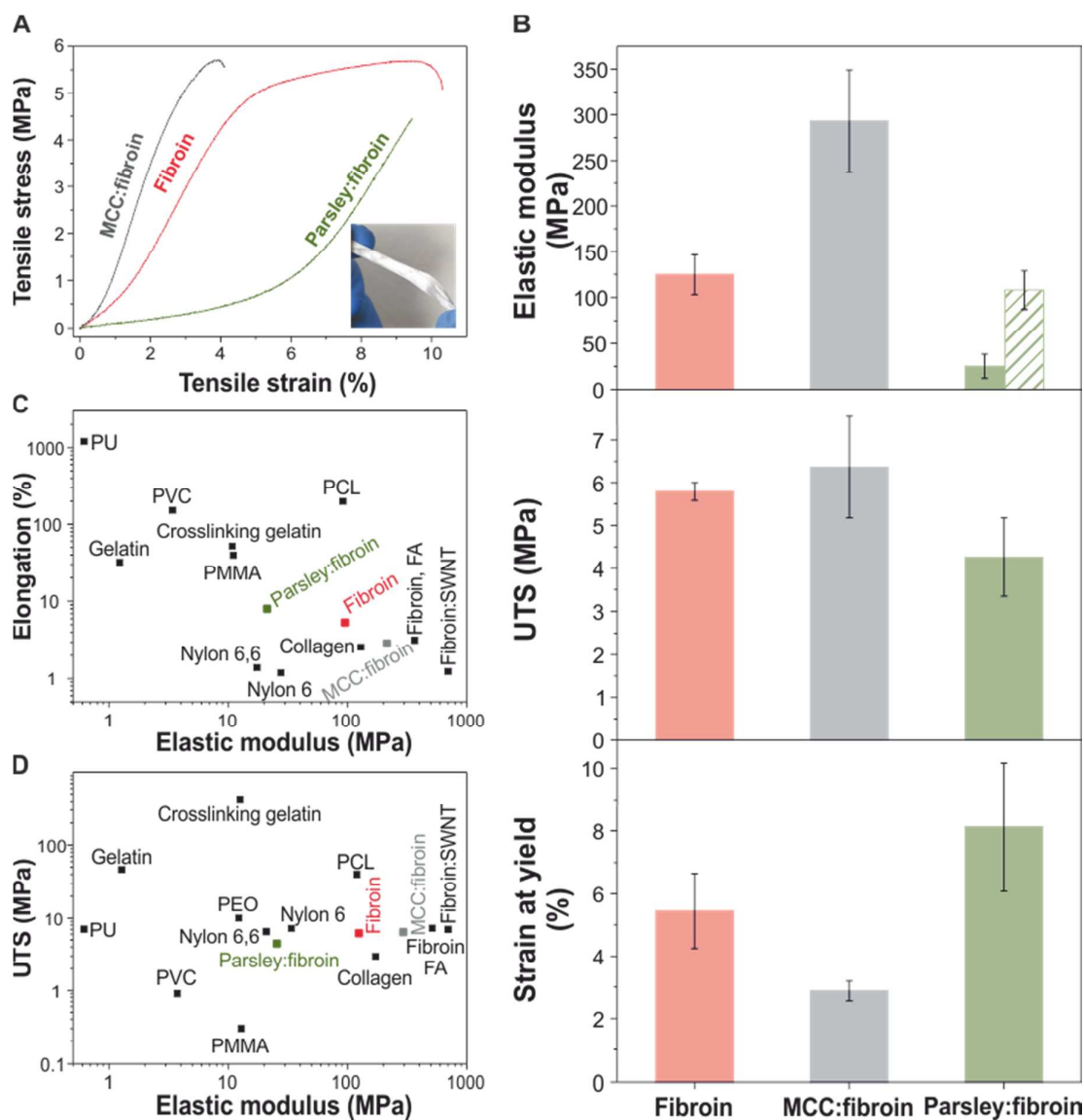
280

281 **Figure 4.** (A) Stress-strain curves of the electrospun nanofibers. Inset: photograph of the nanofibers just after
282 the electrospinning process. (B) Mechanical parameters for the electrospun nanofibers calculated from the
283 stress-strain curves. For parsley:fibroin sample, the two values of elastic modulus corresponding to the two
284 different mechanical behaviors are indicated. (C) Elongation versus elastic modulus data and (D) ultimate
285 tensile strength versus elastic modulus data where other nanofibers prepared using electrospinning are
286 showed.

287

288

| Sample | Apparent elastic modulus (MPa) | Ultimate tensile strength (MPa) | Elongation at yield (%) | Elongation at maximum load (%) |
|---|---|---|---|---|
| Fibroin | 125±21 | 5.8±0.2 | 5.5±1.2 | 10.6±1.7 |
| MCC:fibroin | 293±56 | 6.4±1.2 | 2.9±0.3 | 3.4±0.5 |
| Parsley:fibroin | 22±11<br>108±21 | 4.3±0.9 | 8.1±2.1 | 8.1±2.1 |

289
290 **Table 1.** Mechanical properties (apparent elastic modulus, ultimate tensile strength, elongation at yield and
291 elongation at maximum load) of nanofibers. Data are expressed as mean ± s.d. (n ≥ 5). For parsley:fibroin
292 sample, the two values of elastic modulus corresponding to the two different mechanical behaviors are
293 indicated.

294

295 The obtained stress strain curves can be explained by considering the compositional and

296 morphological differences of the studied materials. The mechanical behavior of pure fibroin mats

297 and their apparent elastic modulus of (125±21) MPa are consistent with previous reports in

298 literature [48]. When fibroin was combined with cellulose a change in the stiffness of the mat was

299 observed, with an increment of the elastic modulus that reached (293±56) MPa for MCC:fibroin

300 nanofibers. Moreover, the strain at yield of the MCC:fibroin samples was lower (~3%) than that one

301 of fibroin sample (~5%); similarly, the elongation at maximum load was negatively affected by the

302 presence of cellulose, with values lower for MCC:fibroin mats (~3%) than for pure fibroin (~11%).

303 It should be noted that the strength was not reduced, suggesting a good mixing of both components.

304 In the case of the parsley:fibroin mats, it is worth noting that their nonlinear behavior is similar to

305 the one of human tendons [49]. For those natural structures, it can be attributed to a crimped

306 waveform organization of the fibers, which is confirmed also for the parsley: fibroin fibers by SEM

307 observations as seen in Figure S2 (supplementary information). The first, low stiffness region,

308 corresponded to the uncoiling of the crimps, enhanced by the low modulus and high flexibility of

14

309    parsley-based material, as already presented in Ref. [37]. The second region behavior most likely

310    starts when most fiber strands are aligned and is mainly ruled by the stiffness of fibroin. The elastic

311    modulus reached a value of (108±21) MPa and the fibers were characterized by a strain at yield of

312    about 8%.

313    A comparison of the mechanical properties of the measured samples with those of other electrospun

314    materials is shown in Figures 4C and 4D [50-56]. Although the effect of the fiber network

315    morphology should be considered for a direct comparison, yet it is possible to appreciate that our

316    blends have a similar stiffness to the one of other natural-based materials, such as fibroin [50] and

317    collagen [51] and comparable values of UTS and elongation of common polymer fibers, such as

318    poly(methyl methacrylate) (PMMA) [52], polyvinyl chloride (PVC) [53], polycaprolactone (PCL)

319    [54] and polyurethane (PU) [53].

320    Considering silk composites, the addition of cellulose has a similar effect, in relative terms, as the

321    addition of single-wall nanotubes (SWNT) in a narrow concentration range [57]. An additional

322    comparison can be made with composites, not produced by electrospinning, based on combinations

323    of fibroin and cellulose (or other polysaccharides), although the sample structure strongly affects

324    the absolute values of mechanical properties. The general modification induced by the addition of

325    cellulose to fibroin is an increment in elongation as well as, to a lesser extent, in strength, while

326    stiffness is usually unaffected [3,12,16,17]. We have, on the contrary, higher stiffness and strength,

327    but a reduction of the tenacity and elongation. We attribute this to the characteristics of MCC

328    obtained through our treatment, stiffer than the one processed by different routes [16, 37, 58].

329    Therefore, when added to fibroin, it acts as reinforcement rather than plasticizer.

330    In order to investigate the structural homogeneity of the produced nanofibers, AFM nanoindentation

331    analysis was conducted in PBS medium (Figure 5). The local stiffness was chosen for such

332    characterization, as it is more sensitive than topology to differentiate different phases even in

333    absence of morphological difference. The maps of the stiffness shown in Figure 5 indicated a

15

334   homogenous and narrow distribution of values in both pure fibroin and hybrid nanofibers, without

335   evident subdomains. This indicates the lack of segregation of the different components and

336   confirms the well mixing and blending for MCC:fibroin and parsley:fibroin nanofibers. The values

337   of stiffness are in agreement with the trend previously discussed for the mats (Figure 4).
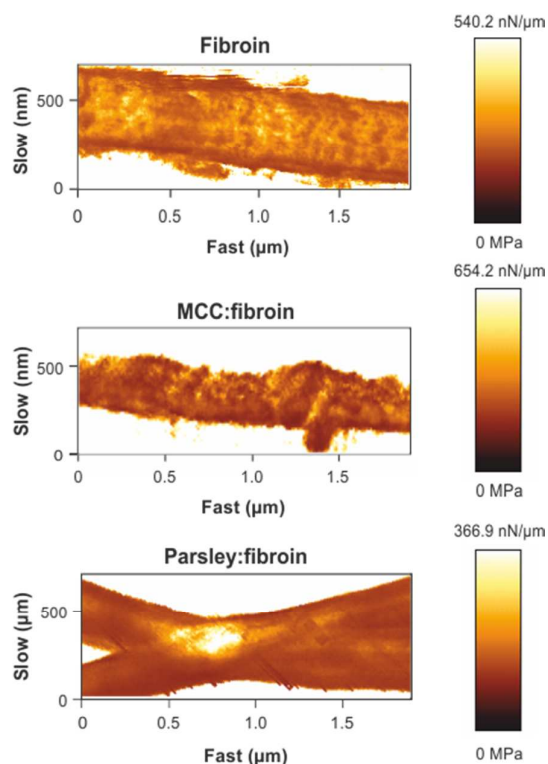
338



339   **Figure 5.** AFM mappings of the electrospun nanofibers showing the indentation stiffness of fibroin,
340   MCC:fibroin and parsley:fibroin nanofibers. The map homogeneity indicates good mixing of the
341   components.

342

**Biocompatibility assays**

343

344   The biocompatibility of the electrospun mats was evaluated using fibroblast cells as *in-vitro* model.

345   Figure 6A shows the MTT results of cell proliferation after 24 hours for the different nanofibrous

346   samples and control (glass substrate). All the prepared nanofibers (pure fibroin, MCC:fibroin and

347   parsley:fibroin) exhibited excellent cell compatibility (higher than the control) and no cytotoxic

348   effects. This verifies that the use of TFA was not detrimental for the cells. Indeed, the acid

349   completely evaporated during the ES process, as demonstrated by ATR-FTIR spectroscopy (Figure

350   3A). Morphological analysis pointed out that the fibroblast cells attached well and spread on the

16

351    electrospun mats nanofibers (Figure 6B-6G). This is also due to the nanometric size of the fibers

352    and their 3D organization that both promote cell proliferation by mimicking the fibrillary

353    topography and high surface area of the native extracellular matrix (ECM) [28]. It is important also

354    to be considered that, in general terms, the chemical composition of the here developed composite

355    fibers of protein and polysaccharide recalls the one of ECM. In fact, in tissues and organs, ECM is a

356    combination of several molecules including proteins (such as collagen and elastin), polysaccharides

357    (such as hyaluronan and chondroitins), proteoglycans, and adhesive glycoproteins [59].

358
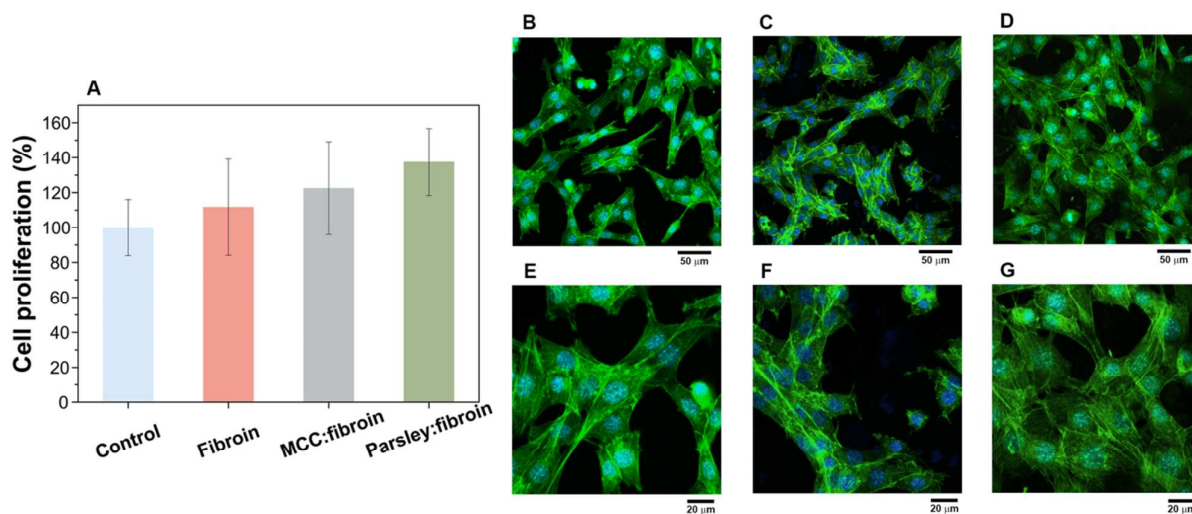
359



360    **Figure 6.** Viability of fibroblast cells (MTT assay) on the different types of nanofibers. Mean ± standard
361    deviation (n = 3) (A). Fluorescence micrographs of fibroblast cells cultured on (B, E) fibroin, (D, F)
362    MCC:fibroin and (D, G) parsley:fibroin nanofibers.

363

## Conclusions

365    In conclusion, we used TFA to codissolve fibroin and cellulose-based materials (pure cellulose and

366    dried powder of parsley stem residues) and to produce hybrid nanofibers (MCC:fibroin and

367    parsley:fibroin) by electrospinning. The choice of TFA as single solvent allowed us to prepare

368    highly mixed blends and, consequently, to avoid phase separation effects in the final nanofibers, as

369    confirmed by morphological and mechanical analysis. In particular, AFM nanoindentation tests

370    demonstrated a uniform distribution of the diverse components inside the nanofibers, without the

17

371    presence of domains having different properties. No cytotoxic byproducts were formed due to the

372    use of TFA, allowing applying the electrospun mats as scaffolds for promoting the proliferation of

373    fibroblast cells. Especially, parsley:fibroin mats showed excellent biocompatibility, probably due to

374    the proper combination of nanoscale topography and mechanical flexibility. The here-discussed

375    method for blending together fibroin and cellulose-based materials and for processing them by ES

376    can be extended to other naturally-derived polymers, creating novel systems for biomedical

377    applications. Moreover, the possibility to process vegetable residues containing cellulose is

378    attractive in view of the valorization and sustainable management of food waste.

379

## Supplementary information

381    Deconvolution of amide I absorption for fibroin, MCC:fibroin, and parsley:fibroin nanofibers and

382    SEM image of parsley:fibroin nanofibers. This material is free of charge via the Internet at

383    http://pubs.acs.org.

384

## Notes

386    The authors declare no competing financial interest.

387

## <u>Acknowledgements</u>

394

## <u>References</u>

18

396   [1] Fratzl, P.; Weinkamer, R. Nature's hierarchical materials. *Progress in Materials Science* **2007**,

397   *52*, 1263-1334.

398   [2] Xu, M; Lewis, R.V. Structure of a protein superfiber: Spider dragline silk. *Proc. Natl. Acad. Sci.*

399   *USA* **1990**, *87*, 7120-7124.

400   [3] Ude, A.U.; Eshkoor, R.A.; Zulkifili, R.; Ariffin, A.K.; Dzuraidah, A.W.; Azhari, C.H. Bombyx

401   mori silk fibre and its composite: A review of contemporary developments. *Materials and Design*

402   **2014**, *57*, 298-305.

403   [4] Chen, F.; Porter, D.; Vollrath, F. Structure and physical properties of silkworm cocoons. *J. R.*

404   *Soc. Interface* **2012**, *9*, 2299-2308.

405   [5] Cosgrove, D.J. Growth of the plant cell wall. *Nature Reviews* **2005**, *6*, 850-861.

406   [6] Marga, F.; Grandbois, M.; Cosgrove, D.J.; Baskin, T.I. Cell wall extension results in the

407   coordinate separation of parallel microfibrils: evidence from scanning electron microscopy and

408   atomic force microscopy. *The Plant Journal* **2005**, *43*, 181-190.

409   [7] Bledzki, A.K.; Gassan, J. Composites reinforced with cellulose based fibres. *Prog. Polym. Sci.*

410   **1999**, *24*, 221-274.

411   [8] Hardy, J.G.; Scheibel, T.R. Composite materials based on silk proteins. *Prog. Polym. Sci.*

412   **2010**, *35*, 1093-1115.

413   [9] Shang, S.; Zhu, L.; Fan, J. Physical properties of silk fibroin/cellulose blend films regenerated

414   from the hydrophilic ionic liquid. *Carbohyd. Polym.* **2011**, *86*, 462-468.

415   [10] Singh, N.; Rahatekar, S.S.; Koziol, K.K.K.; Ng, T.H.S.; Patil, A.J.; Mann, S.; Hollander, A.P.;

416   Kafienah, W. Directing Chondrogenesis of Stem Cells with Specific Blends of Cellulose and Silk.

417   *Biomacromolecules* **2013**, *14*, 1287-1298.

418   [11] Zhou, L.; Wang, Q.; Wen, J.; Chen, X. Shao, Z. Preparation and characterization of transparent

419   silk fibroin/cellulose blend films. *Polymer* **2013**, *54*, 5035-5042.

420 [12] Freddi, G.; Romanò, M.; Massafra, M.R.; Tsukada, M. Silk fibroin/cellulose blend films:

421 preparation, structure, and physical properties. *Journal of applied polymer science* **1995**, *56*, 1537-

422 1545.

423 [13] Yang, G.; Zhang, L.; Liu, Y. Structure and microporous formation of cellulose/silk fibroin

424 blend membranes: I. Effect of coagulants. *Journal of membrane science* **2000**, *177*, 153-161.

425 [14] Yang, G.; Zhang, L.; Cao, X.; Liu, Y. Structure and microporous formation of cellulose/silk

426 fibroin blend membranes: Part II. Effect of post-treatment by alkali. *Journal of membrane science*

427 **2002**, *210*, 379-387.

428 [15] Sashina, E.; Janowska, G.; Zaborski, M.; Vnuchkin, A. Compatibility of fibroin/chitosan and

429 fibroin/cellulose blends studied by thermal analysis. *Journal of Thermal Analysis and Calorimetry*

430 **2007**, *89*, 887-891.

431 [16] Hirano, S.; Nakahira, T.; Zhang, M.; Nakagawa, M.; Yoshikawa, M.; Midorikawa, T. Wet-

432 spun blend biofibers of cellulose-silk fibroin and cellulose-chitin-silk fibroin. *Carbohyd. Polym.*

433 **2002**, *47*, 121-124.

434 [17] Marsano, E.; Canetti, M.; Conio, G.; Corsini, P.; Freddi, G. Fibers Based on Cellulose-Silk

435 Fibroin Blend. *J. Appli. Polym. Sci.* **2007**, *104*, 2187-2196.

436 [18] Yao, Y.; Zhang, E.; Xia, X.; Yu, J.; Wu, K.; Zhang, Y.; Wang, H. Morphology and properties

437 of cellulose/silk fibroin blend fiber prepared with 1-butyl-3-methylimidazolium chloride as solvent.

438 *Cellulose* **2015**, *22*, 625-635.

439 [19] Marsano, E.; Corsini, P.; Canetti, M.; Freddi, G. Regenerated cellulose-silk fibroin blends

440 fibers. *Int. J. Biol. Macromol.* **2008**, *43*, 106-114.

441 [20] Zhang, L.; Webster, T.J. Nanotechnology and nanomaterials: Promises for improved tissue

442 regeneration. *Nano Today* **2009**, *4*, 66-80.

443 [21] Braghirolli, D.I.; Steffens, D.; Pranke, P. Electrospinning for regenerative medicine: a review

444 of the main topics. *Drug Discov. Today* **2014**, *19*, 743-753.

20

445    [22] Wang, X.; Ding, B.; Li, B. Biomimetic electrospun nanofibrous structures for tissue

446    engineering. *Mater. Today* **2013**, *16*, 229-241.

447    [23] Pelipenko, J.; Kocbek, P.; Govedarica, B.; Rošic, R.; Baumgartner, S.; Kristl, J. The

448    topography of electrospun nanofibers and its impact on the growth and mobility of keratinocytes.

449    *Eur. J. Pharm. Biopharm.* **2013**, *84*, 401-411.

450    [24] Liu, W.; Thomopoulos, S.; Xia, Y. Electrospun Nanofibers for Regenerative Medicine. *Adv.*

451    *Healthc. Mater.* **2012**, *11*, 10-25.

452    [25] Khan, F.; Ahmad, S.R. Polysaccharides and Their Derivatives for Versatile Tissue Engineering

453    Application. *Macromol. Biosci.* **2013**, *13*, 395-421.

454    [26] Hajiali, H.; Heredia-Guerrero, J.A.; Liakos, I.; Athanassiou, A.; Mele, E. Alginate nanofibrous

455    mats with adjustable degradation rate for regenerative medicine. *Biomacromolecules* **2014**, *16*, 936-

456    943.

457    [27] Liakos, I.; Rizzello, L.; Hajiali, H.; Brunetti, V.; Carzino, R.; Pompa, P.P.; Athanassiou, A.;

458    Mele, E. Fibrous wound dressings encapsulating essential oils as natural antimicrobial agents. *J.*

459    *Mater. Chem. B* **2015**, *3*, 1583-1589.

460    [28] Zhang, X.; Reagan, M.R.; Kaplan, D.L. Electrospun silk biomaterial scaffolds for regenerative

461    medicine. *Adv. Drug Deliver. Rev.* **2009**, *61*, 988-1006.

462    [29] Kundu, B.; Rajkhowa, R.; Kundu, S.C.; Wang, X. Silk fibroin biomaterials for tissue

463    regenerations. *Adv. Drug Deliver. Rev.* **2013**, *65*, 457-470.

464    [30] Hodgkinson, T.; Chen, Y.; Bayat, A.; Yuan, X.F. Rheology and Electrospinning of

465    Regenerated Bombyx mori Silk Fibroin Aqueous Solutions. *Biomacromolecules* **2014**, *15*, 1288-

466    1298.

467    [31] Jiang, N.; Huang, X.; Li, Z.; Song, L.; Wang, H.; Xu, Y.; Saho, H.; Zhang, Y. Silk fibroin

468    tissue engineering scaffolds with aligned electrospun fibers in multiple layers. *RSC Adv.* **2014**, *4*,

469    47570-47575.

21

470    [32] Jin, H.J.; Fridrikh, S.V.; Rutledge, G.C.; Kaplan, D.L. Electrospinning Bombyx mori silk with

471    poly (ethylene oxide). *Biomacromolecules* **2002**, *3*, 1233-1239.

472    [33] Yao, J.; Masuda, H.; Zhao, C.; Asakura, T. Artificial Spinning and Characterization of Silk

473    Fiber from Bombyx m ori Silk Fibroin in Hexafluoroacetone Hydrate. *Macromolecules* **2002**, *35*, 6-

474    9.

475    [34] Kaefer, C.M.; Milner, J.A. The role of herbs and spices in cancer prevention. *J. Nutr. Biochem.*

476    **2008**, *19*, 347-361.

477    [35] Luthria, D.L. Influence of experimental conditions on the extraction of phenolic compounds

478    from parsley (Petroselinum crispum) flakes using a pressurized liquid extractor. *Food Chem.*

479    **2008**, *107*, 745-752.

480    [36] Kuriyama, I.; Musumi, K.; Yonezawa, Y.; Takemura, M.; Maeda, N.; Iijima, H.; Hada, T.;

481    Yoshida, H.; Mizushina, Y. Inhibitory effects of glycolipids fraction from spinach on mammalian

482    DNA polymerase activity and human cancer cell proliferation. *J. Nutr. Biochem.* **2005**, *16*, 594-601.

483    [37] Bayer, I.S.; Guzman-Puyol, S.; Heredia-Guerrero, J.A.; Ceseracciu, L.; Pignatelli, F.; Ruffilli,

484    R.; Cingolani, R.; Athanassiou, A. Direct Transformation of Edible Vegetable Waste into

485    Bioplastics. *Macromolecules* **2014**, *47*, 5135-5143.

486    [38] Romano, I.; Mele, E.; Heredia-Guerrero, J.A.; Ceseracciu, L.; Hajiali, H.; Goldoni, L.; Marini,

487    L.; Athanassiou, A. Photo-polymerisable electrospun fibres of N-methacrylate glycol chitosan for

488    biomedical applications. *RSC Adv.* **2015**, *31*, 24723-24728.

489    [39] Hutter, J.L.; Bechhoefer, J. Calibration of Atomic-Force Microscope tips. *Rev. Sci. Instrum.*

490    **1993**, *64*, 1868-1873.

491    [40] Seguezza, S.; Dante, S.; Diaspro, A.; Canale C. High resolution nanomechanical

492    characterization of multi-domain model membranes by fast Force Volume. *J. Mol. Recog.* **2015**.

493    DOI: 10.1002/jmr.2490.

494    [41] Goormaghtigh, E.; Cabiaux, V.; Ruysschaert, J.M. Determination of Soluble and Membrane

495    Protein Structure by Fourier Transform Infrared Spectroscopy. In *Physicochemical Methods in the*

22

496 *Study of Biomembranes Subcellular Biochemistry*; Hilderson, H.J.; Ralston, G.B., Eds.; Springer,

497 US, 1994; p 329.

498 [42] Sionkowska, A.; Planecka, A. Preparation and characterization of silk fibroin/chitosan

499 composite sponges for tissue engineering. *J. Mol. Liq.* **2013**, *178*, 5-14.

500 [43] Garside, P.; Wyeth, P. Identification of cellulosic fibres by FTIR spectroscopy - Thread and

501 single fibre analysis by attenuated total reflectance. *Stud. Conserv.* **2003**, *48*, 269-275.

502 [44] Hu, X.; Kaplan, D.; Cebe, P. Determining beta-sheet crystallinity in fibrous proteins by thermal

503 analysis and infrared spectroscopy. *Macromolecules* **2006**, *39*, 6161-6170.

504 [45] Ha, S. W.; Tonelli, A.E.; Hudson, S.M. Structural studies of Bombyx mori silk fibroin during

505 regeneration from solutions and wet fiber spinning. *Biomacromolecules* **2005**, *6*, 1722-1731.

506 [46] Nam, J.; Park, Y.H. Morphology of regenerated silk fibroin: Effects of freezing temperature,

507 alcohol addition, and molecular weight. *J. Appl. Polym. Sci.* **2001**, *81*, 3008-3021.

508 [47] Cestari, M.; Muller, V.; Rodrigues, J.H.D.; Nakamura, C. V.; Rubira, A. F.; Muniz, E. C.

509 Preparing Silk Fibroin Nanofibers through Electrospinning: Further Heparin Immobilization toward

510 Hemocompatibility Improvement. *Biomacromolecules* **2014**, *15*, 1762-1767.

511 [48] Nogueira, G.M.; Rodas, A.C.D.; Leite, C.A.P.; Giles, C.; Higa, O.Z.; Polakiewicz, B.; Beppu,

512 M.M. Preparation and characterization of ethanol-treated silk fibroin dense membranes for

513 biomaterials application using waste silk fibers as raw material. *Bioresource Technol.* **2010**, *101*,

514 8446-8451.

515 [49] Woo, S.L.; Gomez, M.A.; Seguchi, Y.; Endo, C.M.; Akeson, W.H. Measurement of

516 mechanical properties of ligament substance from a bone-ligament-bone preparation. *J. Orthop.*

517 *Res.* **1983**, *1*, 22-9.

518 [50] Ayutsede, J.; Gandhi, M.; Sukigara, S.; Micklus, M.; Chen, H. E.; Ko, F. Regeneration of

519 Bombyx mori silk by electrospinning. Part 3: characterization of electrospun nonwoven mat.

520 *Polymer* **2005**, *46*, 1625-1634.

521  [51] Shields, K. J.; Beckman, M. J.; Bowlin, G. L.; Wayne, J. S. Mechanical properties and cellular

522  proliferation of electrospun collagen type II. *Tissue Eng.* **2004**, *10*, 1510-1517.

523  [52] Carrizales, C.; Pelfrey, S.; Rincon, R.; Eubanks, T. M.; Kuang, A.; McClure, M. J.; Bowlin, G.

524  L.; Macossay, J. Thermal and mechanical properties of electrospun PMMA, PVC, Nylon 6, and

525  Nylon 6,6. *Polym. Advan. Technol.* **2008**, *19*, 124-130.

526  [53] Lee, K. H.; Kim, H. Y.; Ryu, Y. J.; Kim, K. W.; Choi, S. W. Mechanical behavior of

527  electrospun fiber mats of poly(vinyl chloride)/polyurethane polyblends. *J. Polym. Sci. Pol. Phys.*

528  **2003**, *41*, 1256-1262.

529  [54] Tan, E.P.S.; Ng, S.Y.; Lim, C.T. Tensile testing of a single ultrafine polymeric fiber.

530  *Biomaterials* **2005**, *26*, 1453-1456.

531  [55] Zhang, Y.Z.; Venugopal, J.; Huang, Z.M.; Lim, C.T.; Ramakrishna, S., Crosslinking of the

532  electrospun gelatin nanofibers. *Polymer* **2006**, *47*, 2911-2917.

533  [56] Ojha, S.S.; Stevens, D.R.; Stano, K.; Hoffman, T.; Clarke, L. I.; Gorga, R.E. Characterization

534  of electrical and mechanical properties for coaxial nanofibers with poly(ethylene oxide) (PEO) core

535  and multiwalled carbon nanotube/PEO sheath. *Macromolecules* **2008**, *41*, 2509-2513.

536  [57] Ayutsede, J.; Gandhi, M.; Sukigara, S.; Ye, H.; Hsu, C.M., Gogotsi, Y.; Ko, F. Carbon

537  nanotube reinforced Bombyx mori silk nanofibers by the electrospinning

538  process. *Biomacromolecules* **2006**, *7*, 208-214.

539  [58] Guzman-Puyol, S.; Ceseracciu, L.; Heredia-Guerrero, J.A.; Anyfantis, G.C.; Cingolani, R.;

540  Athanassiou, A.; Bayer, I.S. (2015). Effect of trifluoroacetic acid on the properties of polyvinyl

541  alcohol and polyvinyl alcohol–cellulose composites. *Chem. Eng. J.* **2015**, *277*, 242-251.

542  [59] Rosso, F.; Giordano, A.; Barbarisi, M.; Barbarisi, A. From cell-ECM interactions to tissue

543  engineering. *J. Cell. Physiol.* **2004**, *199*, 174-180.

544

545  **Table legend**

546 **Table 1.** Mechanical properties (apparent elastic modulus, ultimate tensile strength, elongation at yield and

547 elongation at maximum load) of nanofibers. Data are expressed as mean ± s.d. (n ≥ 5). For parsley:fibroin

548 sample, the two values of elastic modulus corresponding to the two different mechanical behaviors are

549 indicated.

## Figure legends

551 **Figure 1.** Schematic of the main components of (A) Bombyx mori cocoon and (B) parsley stem

552 residues, and relative organization at different scales.

553 **Figure 2.** SEM images of the electrospun nanofibers: (A) fibroin, (B) MCC:fibroin and (C)

554 parsley:fibroin. Histograms showing the width distribution of the nanofibers: (D) fibroin, (E)

555 MCC:fibroin and (F) parsley:fibroin.

556 **Figure 3.** (A) ATR-FTIR spectra of the electrospun nanofibers. (B) Contribution to amide (%) from

557 deconvolution of the amide I region of the ATR-FTIR spectra. (C) XRD patterns of the electrospun

558 nanofibers. (D) TGA thermograms and derivative thermogravimetric curves of the electrospun

559 nanofibers.

560 **Figure 4.** (A) Stress-strain curves of the electrospun nanofibers. Inset: photograph of the nanofibers just

561 after the electrospinning process. (B) Mechanical parameters for the electrospun nanofibers calculated from

562 the stress-strain curves. For parsley:fibroin sample, the two values of elastic modulus corresponding to the

563 two different mechanical behaviors are indicated. (C) Elongation versus elastic modulus data and (D)

564 ultimate tensile strength versus elastic modulus data where other nanofibers prepared using electrospinning

565 are showed.
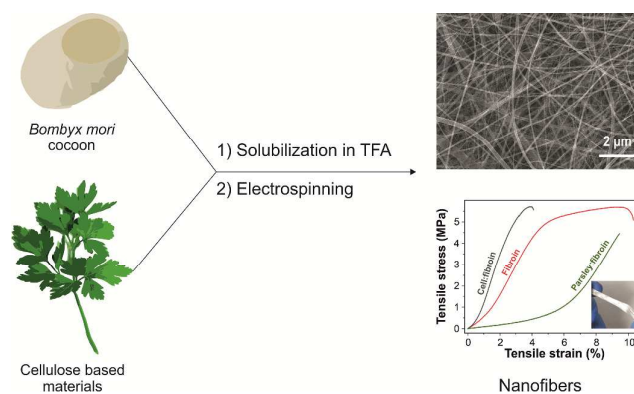
566 **Figure 5.** AFM mappings of the electrospun nanofibers showing the indentation stiffness of fibroin,

567 MCC:fibroin and parsley:fibroin nanofibers. The map homogeneity indicates good mixing of the

568 components.

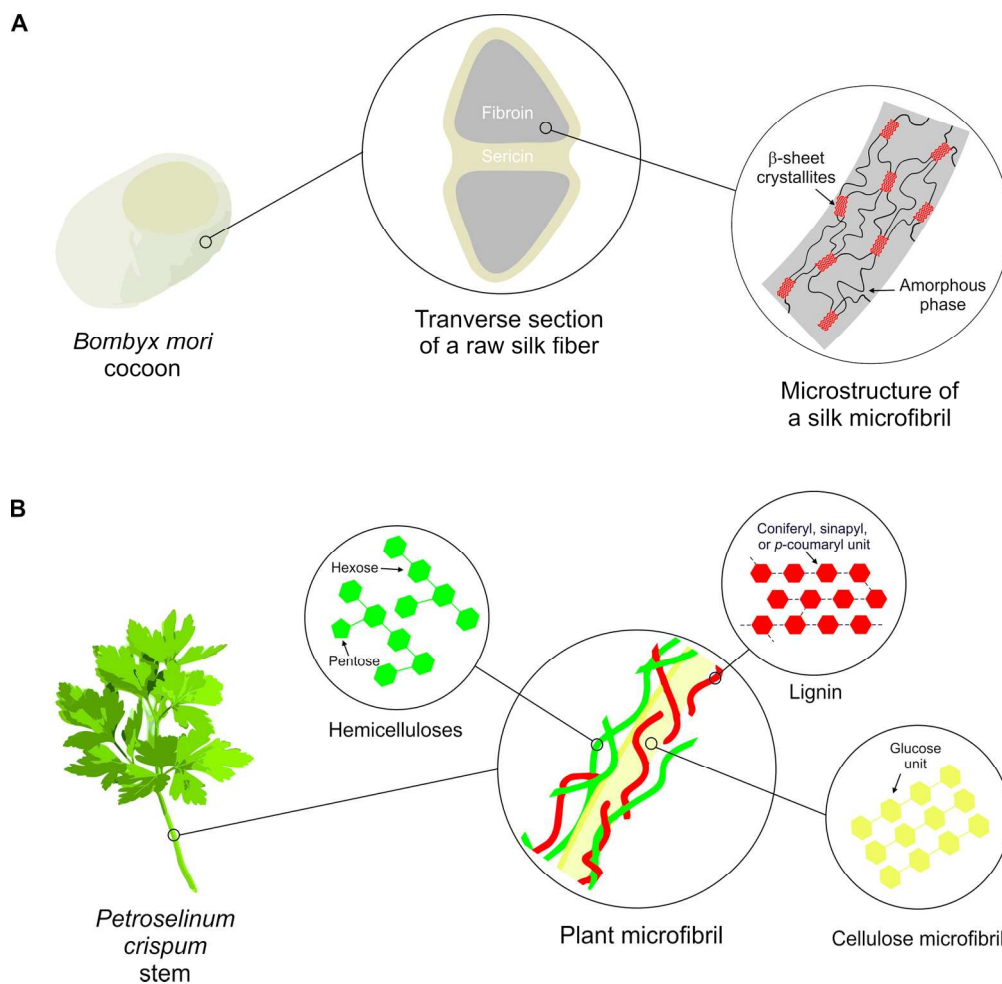569 **Figure 6.** Viability of fibroblast cells (MTT assay) on the different types of nanofibers. Mean ±

570 standard deviation (n = 3) (A). Fluorescence micrographs of fibroblast cells cultured on (B, E)

571 fibroin, (D, F) MCC:fibroin and (D, G) parsley:fibroin nanofibers.

25

572  **Figure   S1.** Deconvolution of amide I absorption for fibroin, MCC:fibroin, and parsley:fibroin

573  nanofibers. Black line represents the real absorption, while color lines represent the different

574  contributions. They are marked as random coil (R), beta-sheets (B), alpha-helices (A), turns (T),

575  and side chains (SC).

576  **Figure   S2.** Detail of the electrospun parsley:fibroin nanofibers showing the crimped waveform

577  organization of the fibers.

578  **Table of Contents Graphic.**



579

1
2
3
4
5
6
7
8
9
10
11
12
13
14
15
16
17
18
19
20
21
22
23
24
25
26
27
28
29
30
31
32
33
34
35
36
37
38
39
40
41
42
43
44
45
46
47
48
49
50
51
52
53
54
55
56
57
58
59
60



Figure 1. Schematic of the main components of (A) Bombyx mori cocoon and (B) parsley stem residues, and relative organization at different scales.
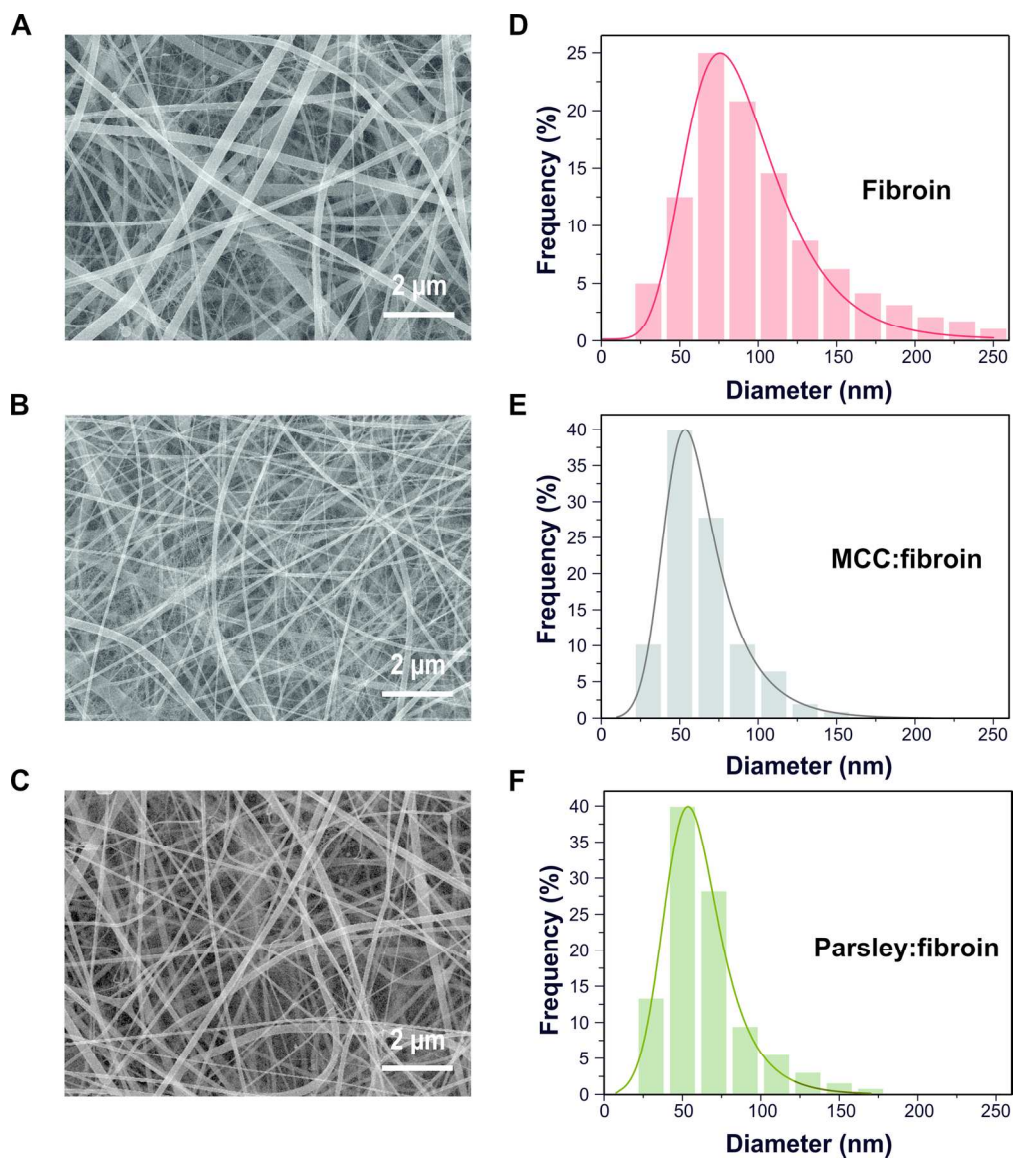159x154mm (300 x 300 DPI)

Figure 2. SEM images of the electrospun nanofibers: (A) fibroin, (B) MCC:fibroin and (C) parsley:fibroin. Histograms showing the width distribution of the nanofibers: (D) fibroin, (E) MCC:fibroin and (F) parsley:fibroin.
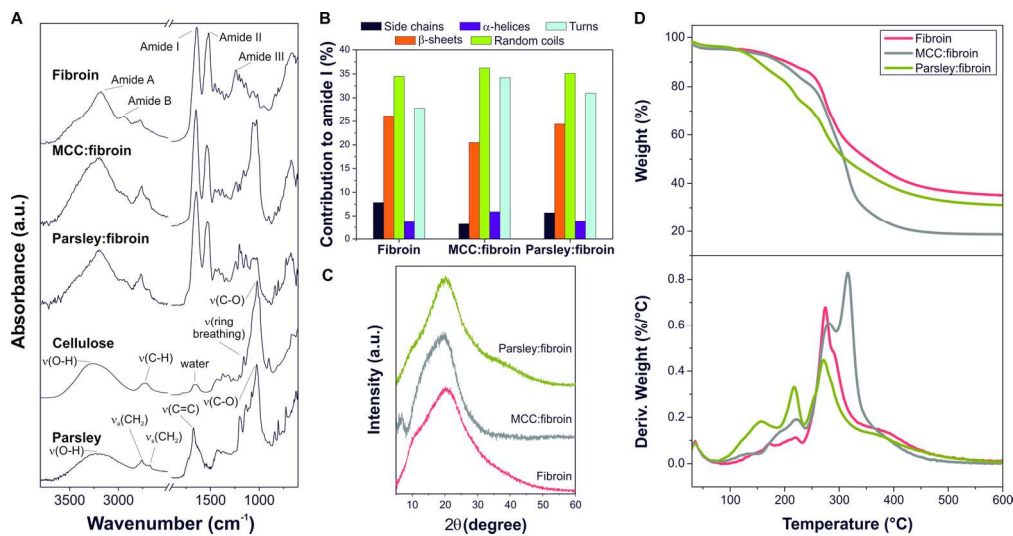167x191mm (300 x 300 DPI)

Figure 3. (A) ATR-FTIR spectra of the electrospun nanofibers. (B) Contribution to amide (%) from deconvolution of the amide I region of the ATR-FTIR spectra. (C) XRD patterns of the electrospun nanofibers. (D) TGA thermograms and derivative thermogravimetric curves of the electrospun nanofibers. 159x82mm (300 x 300 DPI)
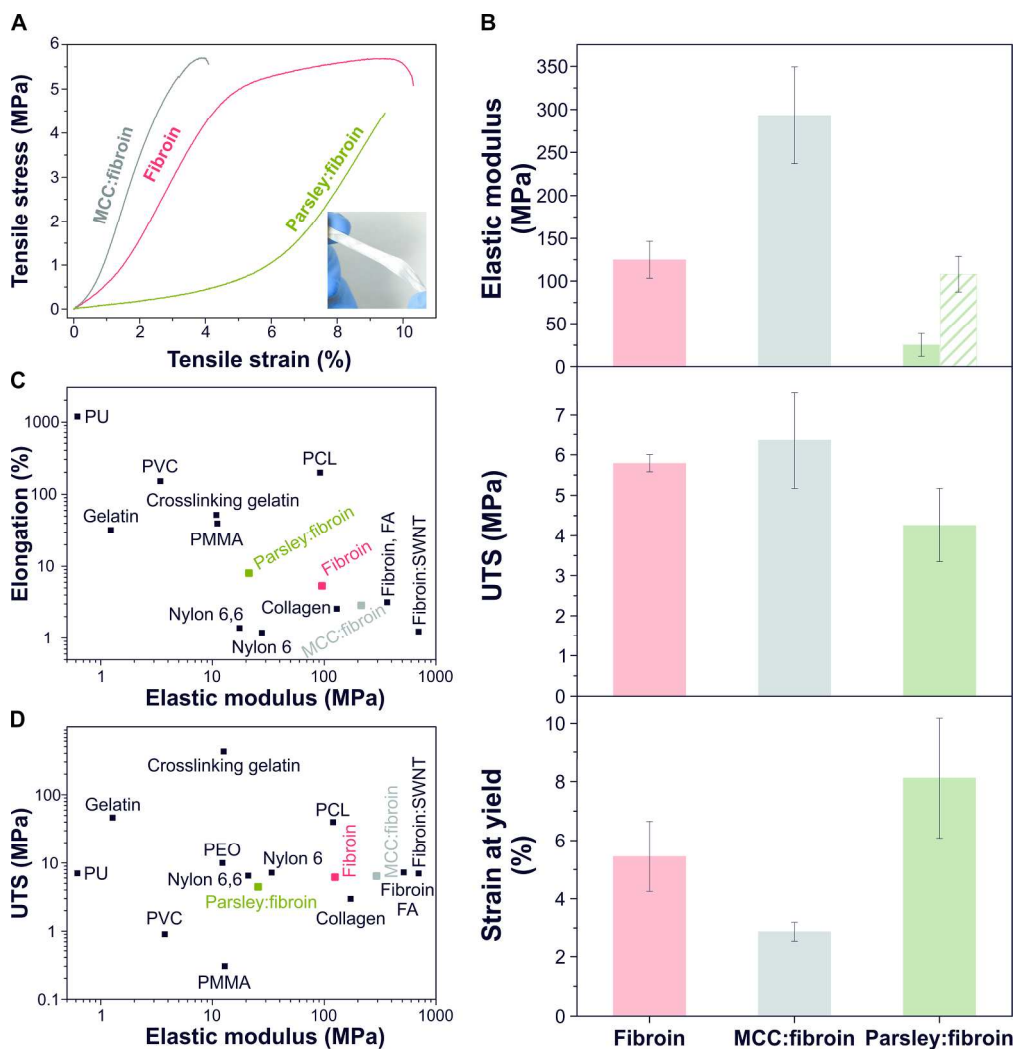
Figure 4. (A) Stress-strain curves of the electrospun nanofibers. Inset: photograph of the nanofibers just after the electrospinning process. (B) Mechanical parameters for the electrospun nanofibers calculated from the stress-strain curves. For parsley:fibroin sample, the two values of elastic modulus corresponding to the two different mechanical behaviors are indicated. (C) Elongation versus elastic modulus data and (D) ultimate tensile strength versus elastic modulus data where other nanofibers prepared using electrospinning are showed.
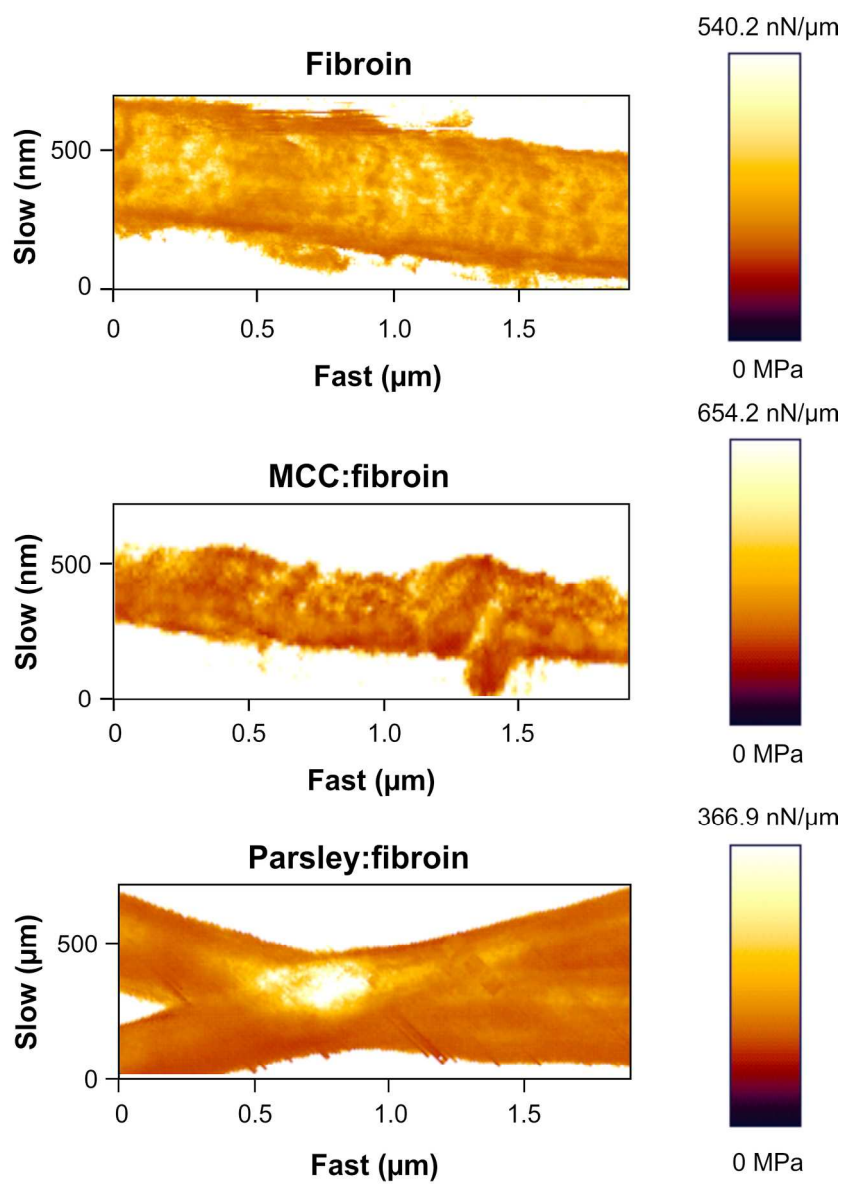
228x236mm (300 x 300 DPI)

Figure 5. AFM mappings of the electrospun nanofibers showing the indentation stiffness of fibroin, MCC:fibroin and parsley:fibroin nanofibers. The map homogeneity indicates good mixing of the components.
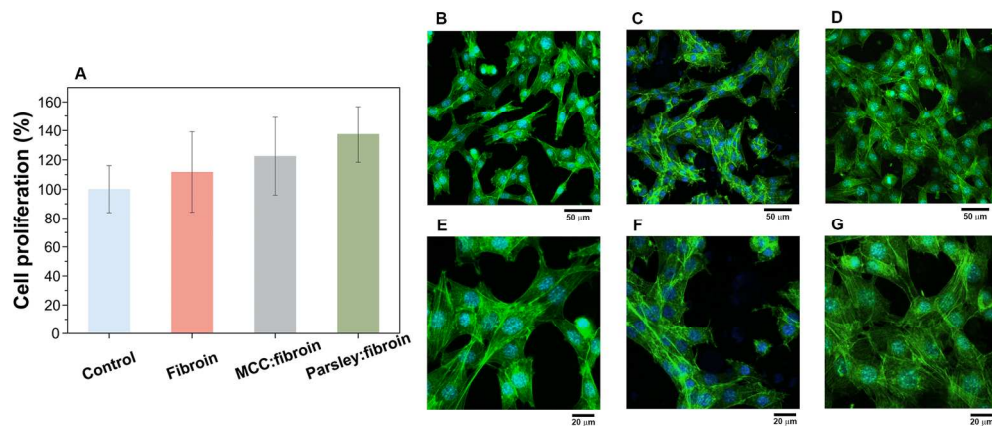160x229mm (300 x 300 DPI)

Figure 6. Viability of fibroblast cells (MTT assay) on the different types of nanofibers. Mean ± standard deviation (n = 3) (A). Fluorescence micrographs of fibroblast cells cultured on (B, E) fibroin, (D, F) MCC:fibroin and (D, G) parsley:fibroin nanofibers.
199x85mm (300 x 300 DPI)